On finite element modeling of compressive failure in brittle materials

J. Cervenka & V. Cervenka
Cervenka Consulting s.r.o., Prague, Czech Republic

S. Laserna
ETSIA, Castilla-La Mancha University, Albacete, Spain

ABSTRACT: Modeling of brittle softening materials requires suitable regularization techniques. This has been long recognized for the modeling of cracking, i.e tensile failure, in brittle materials such as for instance concrete. The crack band approach represents the classical method how to address this problem of proper energy dissipation in the modeling of the tensile failure in the finite element calculation. The paper presents the straightforward extension of this approach for the modeling of compressive failure in brittle materials. This approach was first used in Červenka, et. al. 1998, but more rigorous treatment is necessary and is the subject of this paper.

1 INTRODUCTION

It has been recognized by experimental work by Van Mier 1986 and Tatematsu and Nakamura 1997, 2001 that in compression failure similar size effect as in tensile behavior can be observed. In finite element modeling of brittle materials such as concrete, the compressive behavior is as important as the tensile response. The compressive failure is often a critical behavior, which controls the ultimate limit state of the investigated structure. The regularization techniques for the modeling of cracking in brittle materials have been extensively investigated in the past, and various approaches have been proposed such as: crack band method, nonlocal averaging, higher order continuum theories, etc. All these approaches can be applied to the compressive softening as well, however, it is not usually done, mainly due to the fact that the experimental evidence is limited.

The paper discusses the importance of an appropriate modeling of compressive softening in concrete structures on several examples with experimental data involving compressive crushing of concrete. The crush band approach is proposed for the modeling of the mesh objective energy dissipation during the crushing process. The crush band size is calculated as a finite element size projected into the direction of the minimal principal stress. The crush band size is in addition adjusted based on the finite element shape and the crush band direction.

One example of practical application will be presented, which involves modeling of ultimate limit states and fatigue states in grouted connection in offshore wind farms. In this grouted connection significant tensile and compressive stress concentration occurs, which makes it difficult to use standard design approaches based on checking the stress values. The global assessment based on nonlinear analysis can be successfully applied if proper modeling of the nonlinear effects in the high stress concentration zones is used.

2 MATERIAL MODEL FOR CONCRETE

The emphasis of the paper is on the modeling of compressive failure in brittle materials such as concrete and reinforced concrete. Compressive failure in reinforced concrete structures involves often complex failure mechanism involving cracking, reinforcement yielding, bond failure between concrete and reinforcement as well as compressive crushing. Therefore at least a brief outline of the used material model is necessary. The used material model has been published in more details in Červenka et. al. 1998 and Červenka et. al. 2013.

The material model formulation is based on the decomposition of the strain vector into elastic $\bar{\varepsilon}_e$, plastic $\bar{\varepsilon}_p$ and fracturing $\bar{\varepsilon}_f$ strains, which for the incremental nonlinear solution can be written in the rate form as

$$\dot{\bar{\varepsilon}} = \dot{\bar{\varepsilon}}_e + \dot{\bar{\varepsilon}}_p + \dot{\bar{\varepsilon}}_f \tag{1}$$

The stress evolution is described by the formula:

$$\dot{\bar{\sigma}} = \mathbf{E}(\dot{\bar{\varepsilon}} - \dot{\bar{\varepsilon}}_p - \dot{\bar{\varepsilon}}_f) \tag{2}$$

In the above $\mathbf{E}$ is elastic stiffness and the two unknown strain vectors are defined as:

$$\dot{\bar{\varepsilon}}_f = \frac{\mathbf{E}}{\mathbf{E} + \mathbf{T}^{\mathrm{T}}\mathbf{E}_f\mathbf{T}}\left(\dot{\bar{\varepsilon}} - \dot{\bar{\varepsilon}}_p\right) \tag{3}$$

$$\dot{\bar{\varepsilon}}_p = \dot{\lambda}_p \bar{m}, \quad \dot{\lambda}_p = \frac{\bar{n}^{\mathrm{T}}\mathbf{E}\left(\dot{\bar{\varepsilon}} - \dot{\bar{\varepsilon}}_f\right)}{\bar{n}^{\mathrm{T}}\,\mathbf{E}\,\bar{m} - H_p}, \qquad \bar{n} = \frac{\partial F_p}{\partial \bar{\sigma}}, \quad \bar{m} = \frac{\partial G_p}{\partial \bar{\sigma}} \tag{4}$$

Eq. (3) represents the fracturing model, which takes into account the development of tensile cracks, while the Eq. (4) corresponds to the plasticity model for the modeling of compressive concrete failure. These two equations are not independent and must be solved by an iterative algorithm, which is described in detail in Červenka & Papanikolaou 2008.

In the fracturing model, Eq.(3), the fracturing strain $\dot{\bar{\varepsilon}}_f$ is calculated from the Eq.(2), where $\dot{\bar{\sigma}}$ is replaced by the stress in the cracks as defined in Eq.(5). $\mathbf{T}$ is the strain transformation matrix for transforming the strain vector from the global coordinate system into the local coordinate system aligned with cracks in concrete, and $\mathbf{E}_f$ is the stiffness matrix for the cracks. In the present model, maximum three orthogonal cracks can be modeled at each point and the matrix $\mathbf{E}_f$ has the following form:

$$\dot{\bar{\sigma}}' = \mathbf{E}_f\,\dot{\bar{\varepsilon}}', \qquad \mathbf{E}_f = \begin{bmatrix} {}^{1}E_f & 0 & 0 & & & \\ 0 & {}^{2}E_f & 0 & & \mathbf{0} & \\ 0 & 0 & {}^{3}E_f & & & \\ & & & {}^{12}E_f & 0 & 0 \\ & \mathbf{0} & & 0 & {}^{23}E_f & 0 \\ & & & 0 & 0 & {}^{13}E_f \end{bmatrix} \tag{5}$$

where the prime indicates the stress and strain quantities in the local coordinate system in cracked concrete. The individual components of the matrix E_f are calculated by Eq. (6) using the softening evolution law (Figure 1) for the tensile strength f_t, which is a function of the crack opening displacement w_t. The crack band method of Bažant & Oh 1983 is used, which allows to relate the crack opening displacement w_t to the fracturing strains $\bar{\varepsilon}_f$ through the crack band size L_T (Figure 1). The shear components ${}^{ij}E_f$ of the matrix $\mathbf{E}_f$ are assumed to be dependent on the corresponding normal components and on the multiplier s_F, which is assumed to be an input material parameter.

$${}^{i}E_f = \frac{\partial f_t\left({}^{i}w_t\right)}{\partial w} L_T, \qquad {}^{ij}E_f = s_F \min\left({}^{i}E_f, {}^{j}E_f\right), \quad {}^{i}w_t = {}^{i}\varepsilon_f\, L_T \tag{6}$$

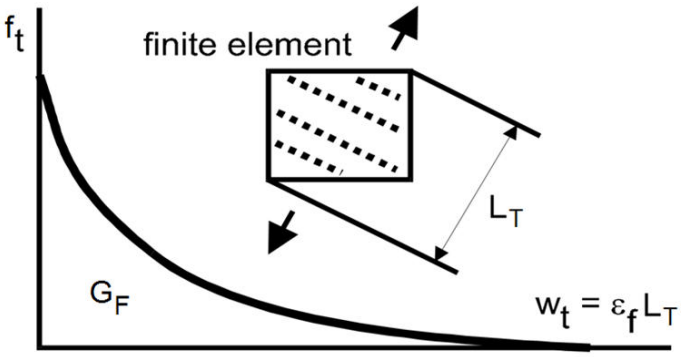

Figure 1: Crack opening law of Hordijk 1991 and crack band L_T.

The elements of the transformation matrix $\mathbf{T}$ are gradually calculated at the onset of cracking in each of the three material directions. This corresponds to the fixed crack model, when the crack direction is fixed after the initiation. On the other hand, if the matrix $\mathbf{T}$ is recalculated for each step based on direction of the current principal strains, a rotated crack model is recovered. It should be also noted that evaluation of the fracturing model, i.e. the Eqs.(3),(6) requires an iterative algorithm since $\mathbf{E}_f$ depends $\bar{\varepsilon}_f$. This algorithm is described in detail in Červenka & Papanikolaou 2008.

In the plasticity model, Eq.(4), the plastic strain rate $\dot{\bar{\varepsilon}}_p$ is calculated from the consistency condition. λ_p is the plastic multiplier, and $\bar{n}$ and $\bar{m}$ are stress derivatives of the plastic and potential surface respectively. The plastic surface F_p is defined by the three-parameter criterion, (f_c, f_t, e), according to Menetrey & Willam 1995 (Figure 2).

$$F_p = \left[\sqrt{1.5}\,\frac{\rho}{f_c}\right]^2 + m\left[\frac{\rho}{\sqrt{6}\,f_c}\,r(\theta, e) + \frac{\xi}{\sqrt{3}\,f_c}\right] - c = 0 \tag{7}$$

$$m = 3\frac{\hat{f}_c^2 - f_t^2}{\hat{f}_c f_t}\frac{e}{e+1}$$

$$r(\theta,e) = \frac{4(1-e^2)\cos^2\theta + (2e-1)^2}{2(1-e^2)\cos\theta + (2e-1)\left[4(1-e^2)\cos^2\theta + 5e^2 - 4e\right]^{\frac{1}{2}}}$$

In the above equations, (ξ,ρ,θ) are the Haigh-Westergaard stress coordinates and f_c and f_t are the compressive strength and tensile strength, respectively. Parameter $e \in (0.5,1.0)$ defines the roundness of the Menétrey-Willam failure surface, with a recommended value e = 0.52. The plastic surface is not constant. Its evolution is governed by the equivalent plastic strain ε_{eqp} (Figure 3):

$$\dot{\varepsilon}_{eqp} = \min\left(\dot{\varepsilon}_{p1}, \dot{\varepsilon}_{p2}, \dot{\varepsilon}_{p3}\right) \tag{8}$$

where ε_{pi} is the i-th component of the principal plastic strains. The hardening is modelled by adjusting the compressive strength $\hat{f}_c$, while the softening is controlled through the parameter c

Hardening $\varepsilon_{eqp} \in \langle -\varepsilon_{cp}; 0 \rangle$

$$\hat{f}_c(\varepsilon_{eqp}) = f_{c0} + (f_c - f_{c0})\sqrt{1 - \left(\frac{\varepsilon_{cp} - \varepsilon_{eqp}}{\varepsilon_{cp}}\right)^2} \tag{9}$$

Softening $\varepsilon_{eqp} \in \langle -\infty; -\varepsilon_{cp} \rangle$

$$c = \left(1 - \frac{w_c}{w_d}\right)^2, \quad w_c \in \langle -w_d; 0 \rangle$$
$$c = 0, \quad w_c \in (-\infty; w_d) \tag{10}$$
$$w_c = (\varepsilon_{eqp} - \varepsilon_{cp})\, L_c$$

In the formulas above, ε_{cp} is the value of the plastic strain when the compression strength f_c is reached in a uni-axial compression test. f_{c0} is the onset of nonlinear behaviour in compression, w_d is the critical value of compressive displacement and w_c is the crushing displacement analogical to crack opening displacement, but with different sign. When concrete crushing enters into the softening regime, an analogous approach to the crack band model is also used for the localization in compression within the crushing band L_c. The crushing band L_c is calculated for each finite element as the element size projected into the direction of the minimal compressive stress (Figure 4). This approach is based on the work of Van Mier 1986, where it was experimentally shown that a unique value of the post-peak critical crushing displacement w_d was recovered for the tested specimens independent of their sizes.

The plastic potential (11) defines the direction of the plastic flow, and is controlled by the parameter β , which defines the volumetric change during the crushing process: $\beta > 0$ means volume expansion, $\beta < 0$ material compaction, $\beta = 1$ material volume is preserved

$$G_p(\bar{\sigma}) = \beta\frac{1}{\sqrt{3}}I_1 + \sqrt{2J_2} \tag{11}$$

I_1 is the 1st invariant of stress vector and J_2 is the 2nd invariant of deviatoric stress vector. The hardening/softening modulus H_p from (4) is defined as

$$H_p = \frac{\partial F_p}{\partial f_c}\frac{\partial f_c}{\partial \varepsilon_{eqp}}\frac{\partial \varepsilon_{eqp}}{\partial \lambda_p} + \frac{\partial F_p}{\partial c}\frac{\partial c}{\partial w_c}\frac{\partial w_c}{\partial \lambda_p} \tag{12}$$

The presented model is used in the examples presented in this paper.

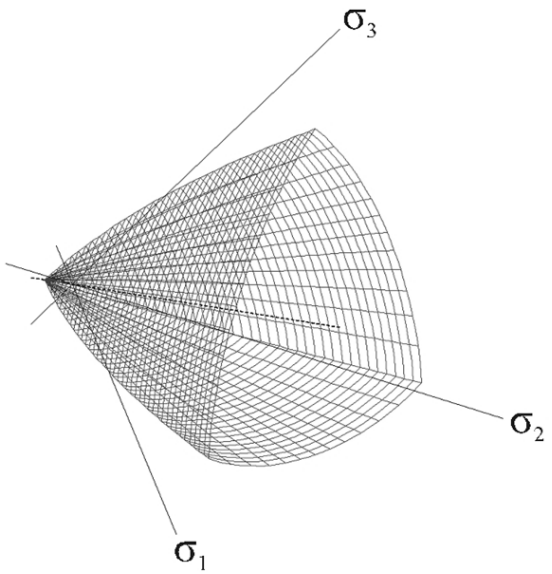

Figure 2. Visualization of the three-parameter Menetrey & Willam 1995 three-parameter concrete failure criterion.

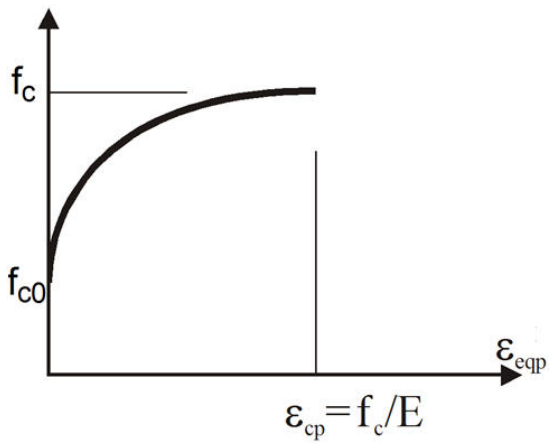

Figure 3. Hardening law for the plasticity model for concrete in compression.

3 MODELING OF COMPRESSIVE SOFTENING

In the presented model, the softening in compression is controlled by the linear law in Figure 4 and Eq. (10), in which the parameter c of the criterion (7) is reduced as a function of the crushing displacement w_c, which has an analogous meaning to the crack opening w_t (Figure 1).

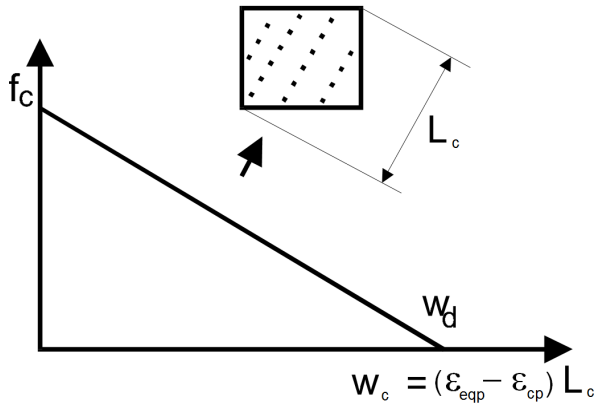

Figure 4. Softening law for the plasticity model for concrete in compression.

Using compression tests of specimens with different sizes it was experimentally documented by Van Mier 1986 and Nakamura & Higai 2001 that a compressive fracture energy exists. This suggests that an analogous approach to the crack band model could be adopted also for modeling softening in compression by the finite element method.

This modeling approach to compression softening has been already introduced by Cervenka J. et. al. 1998 and Cervenka V. & Bergmeister 1999. When this approach is adopted, the crush band size L_c is calculated as the projection of the element size into the direction of the minimal principal stress. This approach can nicely capture the concrete response in compression if the size of the finite element is significantly larger than the size of the zone of the expected compressive localization. This is documented in Figure 9, which shows the response of Nakamura & Higai 2001 experiments of compression cylinders with the same cross-sectional area but with different lengths (Figure 5). The numerical results in Figure 9 were calculated by models with only a single finite element. This is identical to assuming a macroscopic model with only single material point. As can be seen in Figure 9, the results correspond very well with the experimental evidence, and the size effect is correctly reproduced, i.e. the larger specimens exhibit more brittle behavior.

If the same cylindrical tests are, however, modeled with smaller elements (Figure 6) totally incorrect response is recovered. In order to recover the correct responses as shown in Figure 10, it is necessary to use a value of $L_c = 150$ mm in Eq. (10). Interestingly this value corresponds to the diameter of the cylinders, and is also in agreement with the length of the damaged zones reported in Nakamura & Higai 2001, where it approximately corresponds to the diameter of the investigated cylinders.

Based on this it is proposed to introduce a limit on the minimal value for L_c. This $L_c^{\lim}$ is equal to the minimal dimension of the crushed zone.

4 VALIDATION

The assumption of limiting crush band size $L_c^{\lim}$ was tested on the same cylindrical tests of Nakamura & Higai 2001 (Figure 6) using different mesh sizes 15, 30 and 60 mm. Later it was applied to the modeling of bending rotational capacity of reinforced concrete beams (Figure 7).

The results for the cylindrical tests are reported in Figure 10 to Figure 12. It can be seen that the calculated results correctly reproduce the expected increase of brittleness for larger specimens, but the accuracy deteriorates as the element size increases. This is caused by the fact that for element size 60 mm, there are only 2-3 elements across the specimen diameter and in the localization length L_c = 150 mm. This model cannot accurately capture the strain and stress localization as shown in Figure 13 and Figure 14 respectively.

The proposed method was also verified using the reinforced concrete beams tested by Bosco & Debenardi 1993. Accurate modelling of compressive crushing is important for the prediction of rotational capacity of reinforced concrete beams. For beams with low reinforcement ratio, the strength and the rotational capacity is mainly given by the yielding strength of reinforcement and its critical elongation at rupture.

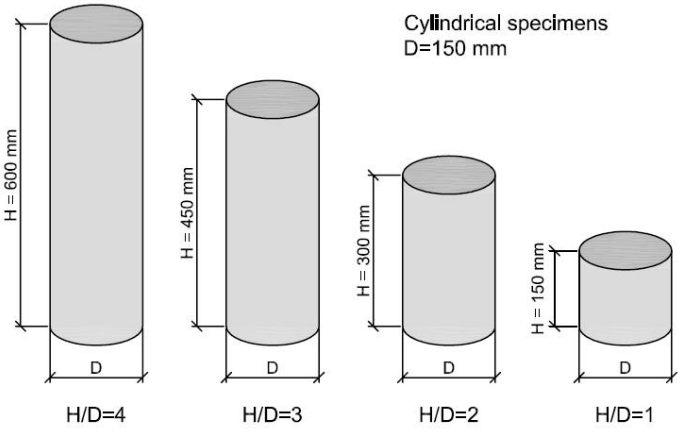

Figure 5: Cylindrical specimens for Nakamura & Higai 2001 tests

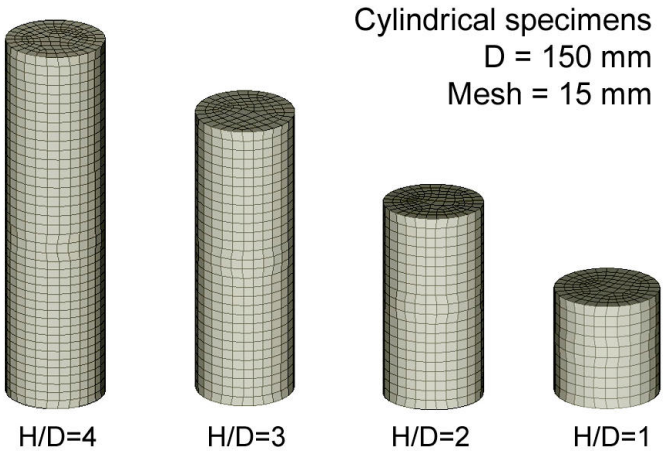

Figure 6: Mesh for cylindrical specimens for Nakamura & Higai 2001 tests.

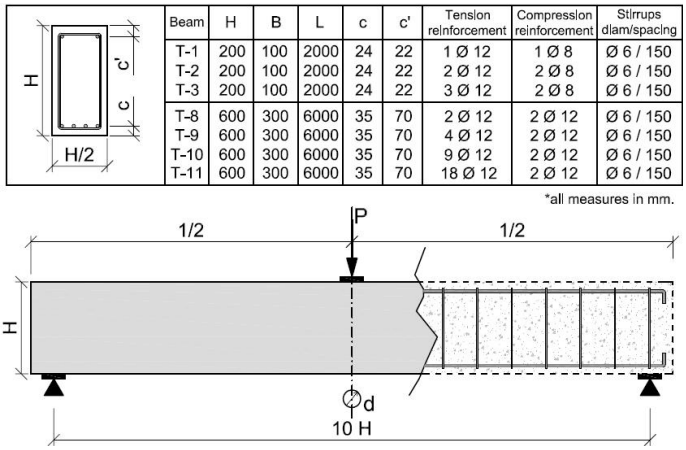

Beam	H	B	L	c	c'	Tension reinforcement	Compression reinforcement	Stirrups diam/spacing
T-1	200	100	2000	24	22	1 Ø 12	1 Ø 8	Ø 6 / 150
T-2	200	100	2000	24	22	2 Ø 12	2 Ø 8	Ø 6 / 150
T-3	200	100	2000	24	22	3 Ø 12	2 Ø 8	Ø 6 / 150
T-8	600	300	6000	35	70	2 Ø 12	2 Ø 12	Ø 6 / 150
T-9	600	300	6000	35	70	4 Ø 12	2 Ø 12	Ø 6 / 150
T-10	600	300	6000	35	70	9 Ø 12	2 Ø 12	Ø 6 / 150
T-11	600	300	6000	35	70	18 Ø 12	2 Ø 12	Ø 6 / 150

*all measures in mm.

Figure 7: Geometry of the beam specimens Bosco & Debenardi 1993

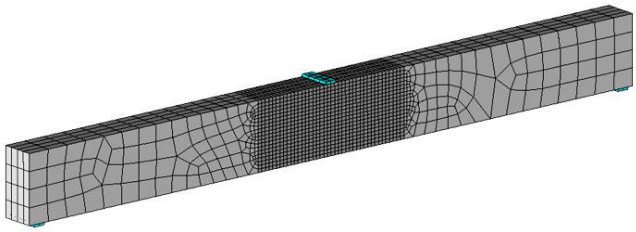

Figure 8: Typical mesh for the beam specimens with mesh size in the middle section 30 mm.

Table 1: Material parameters used in the validation examples

Parameter	Comp. tests on cylinders	Flexural tests on beams
E (MPa)	20 000	22 000
μ	0,2	0,2
f_c (MPa)	20,0	27,8
f_t (MPa)	1,6	2,2
ε_{cp} (mm/mm)	0,002	0,000933
GF (N/m)	125,0	55,0
β	0,5	0,5
w_d (mm)	2,5	2,5

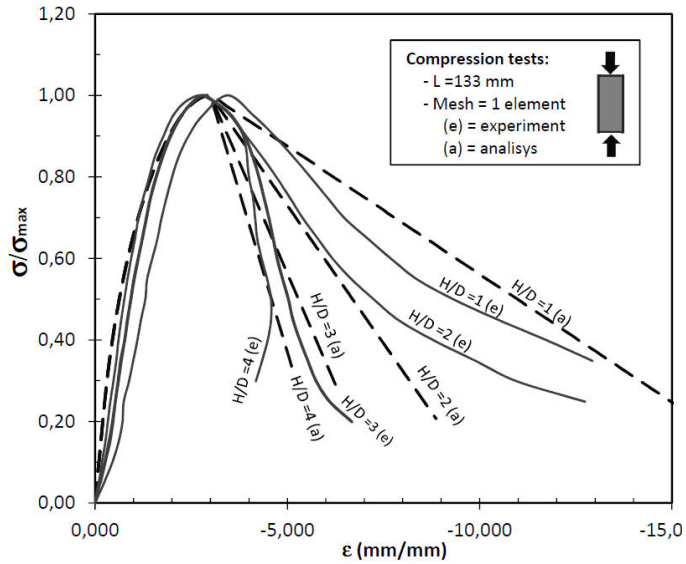

Figure 9: Response curves for single element analyses for different specimen sizes

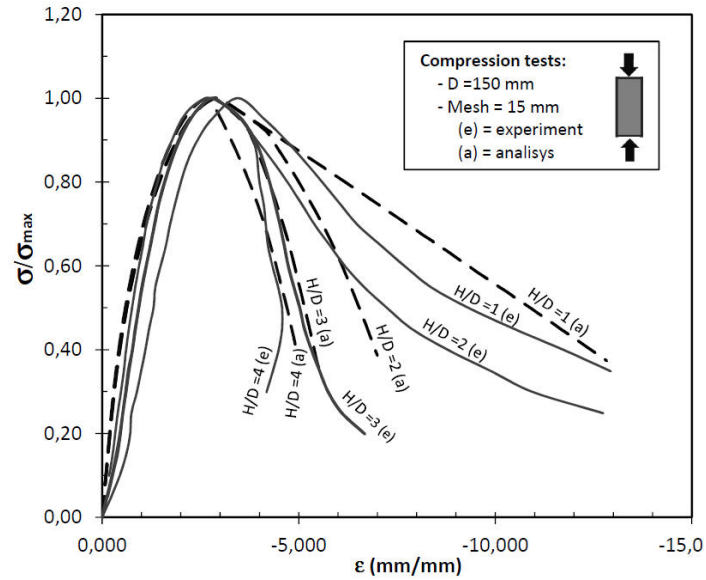

Figure 10: Response curves for cylindrical specimens for element size 15 mm.

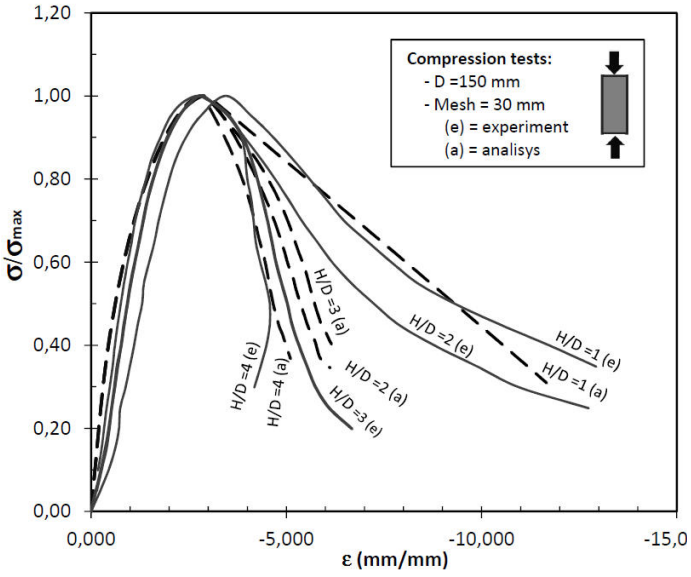

Figure 11: Response curves for cylindrical specimens for element size 30 mm.

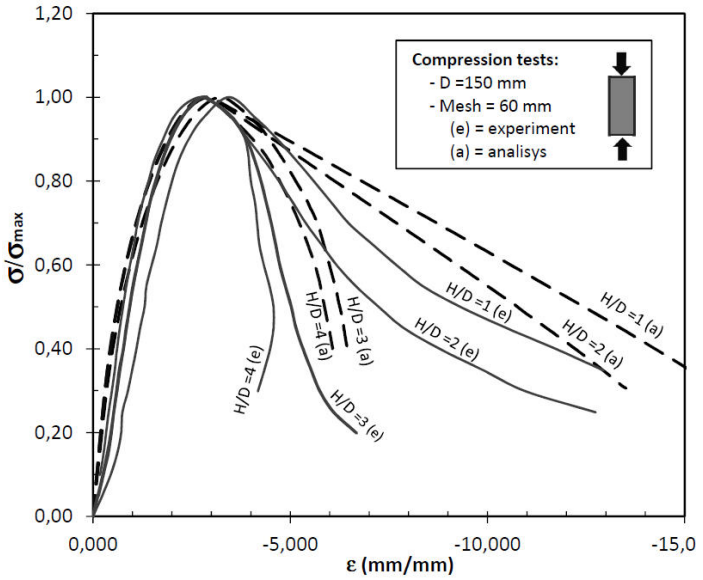

Figure 12: Response curves for cylindrical specimens for element size 60 mm.

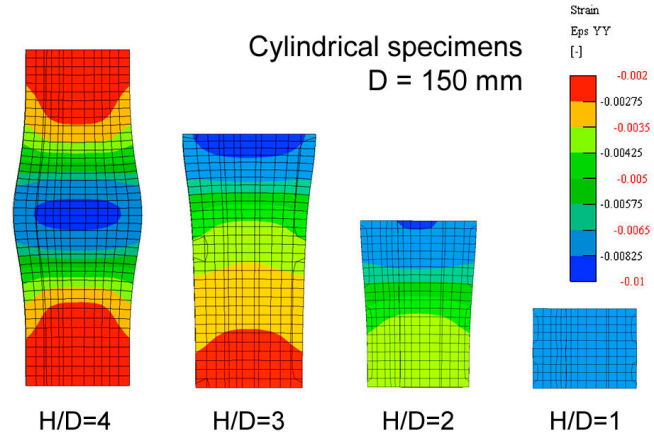

Figure 13: Strain localization in cylindrical specimens for element size 15 mm.

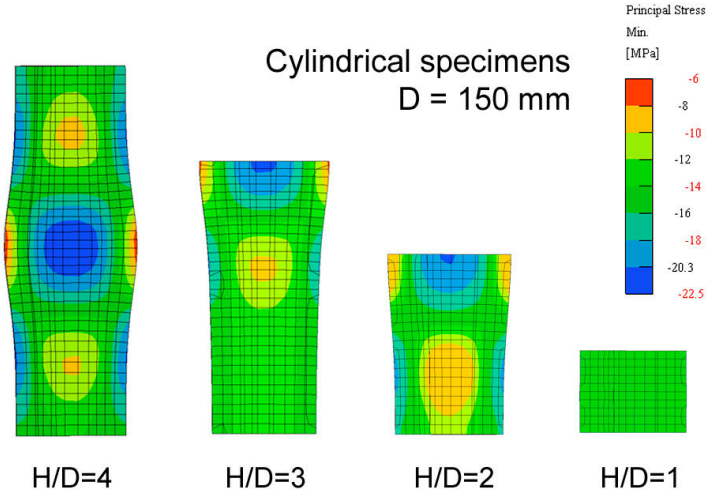

Figure 14: Stress confinement zones in cylindrical specimens for element size 15 mm.

For beams with high reinforcement ratio, the strength as well the rotational capacity is controlled by the capacity of the compressed section to absorb high compressive strains without significant softening.

The experimental results of Bosco & Debenardi 1993 were used to evaluate if the proposed model can correctly repoduce the different failure modes observed in the experiments, i.e. mainly the switch between the reinforcement rupture and concrete crushing mode of failure.

The geometry and reinforcement arrangement of the analyzed beams is described in Figure 7. Two beam dimensions were considered: small beams with the dimension 100x200x2000 mm and larger beams with 300x600x6000 mm. For each beam dimension, several reinforcement ratios are considered, which should demonstrate the switch of the failure mode.

The typical finite element mesh is shown in Figure 8. The reinforcement is modeled using the embedded approach and the bond model by Jendele & Cervenka 2006. For the both beam types the element size in the middle zone was 30 mm. The limiting value of $L_c^{\lim}$ can be estimated by the theoretical size of the compression rectangle based on the equivalence of forces in the bending reinforcement and in the concrete compressed region.

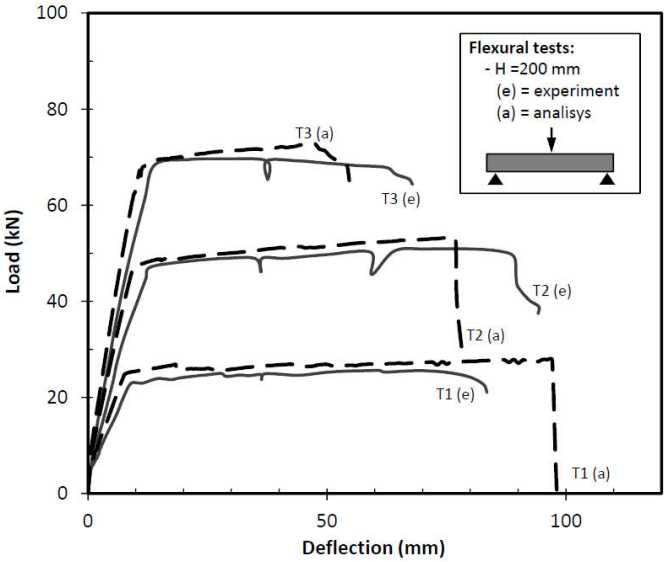

Figure 15: Response curves for small beams.

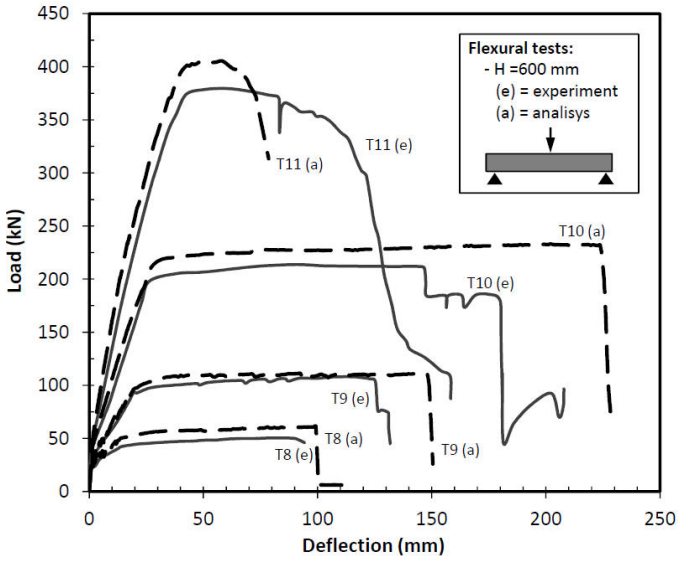

Figure 16: Response curves for big beams.

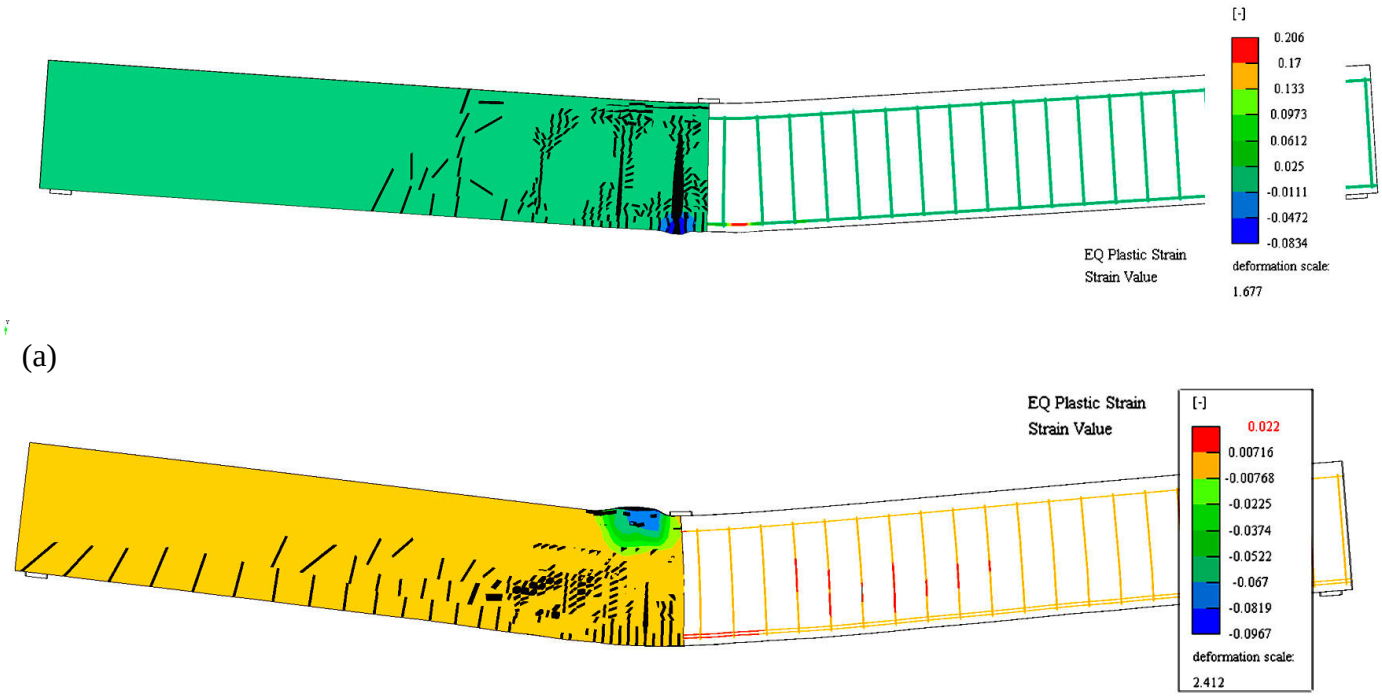

(a)

(b)

Figure 17: Failure mode for big beams with low reinforcement ratio with reinforcement rupture (a) and high reinforcing ratio with concrete crushing (b).

The resulting load-displacement graphs are shown in Figure 15 and Figure 16 for the small and large beams respectively.

The beams with lower reinforcement ratio failed by reinforcement rupture (Figure 17a). This was the case of beams T1-2, T8-10. The reinforcement yield strength was 565 MPa, and tensile strength was 672 MPa at the critical strain of 7%. The concrete crushing (Figure 17b) was observed only for the cases with the highest reinforcement ratio, i.e. beams T3 and T11. The results were obtained assuming the value of $L_c^{\min}$ 38 and 94 mm for T3 and T11 respectively, which is significantly lower than the theoretical values of 108 and 160 mm for T3 and T11 respectively. The theoretical values of the compression zone sizes were calculated assuming the classical distribution of stresses in reinforced concrete section at the ultimate limit state. The graphs for T3 and T11 in Figure 15 and Figure 16 on the other hand shows slightly too brittle response of the numerical model compare to the experimental one. It should be also noted that the post-peak softening was not known for the used concrete type so the same w_d was assumed as in the cylindrical models from the first validation problem.

The problem of compressive softening is still not well understood also from the experimental point of view since the w_d values suggested by the two experimental works by Van Mier 1986 and Nakamura Nakamura & Higai suggests the value of 2.5 mm. It is therefore highly recommended to always validate the model on suitable experimental results before applying it to practical engineering problems. The validation should be always performed using experiments, which show failure modes that are expected in the real structure. This reduces the model uncertainties and increases the reliability of the numerical simulation.

5 APLICATION

Offshore wind farms appear as a fast growing industry in response for demand for renewable energy sources and sustainable energy production. Wind turbines are installed on the top of offshore steel structures located on the sea bed (Figure 18). A tower superstructure is fixed to the foundation piles using technology of grouted connections, in which the ultra high performance concrete (UHPC) is used as a grout material. In this technology the grout is subjected to extremely high load actions, which should be verified by design.

The grout material has a high strength comparable to steel, but exhibits brittleness and fatigue sensitivity. Therefore, the design of grouted connection is aided by numerical simulations, in which real properties of grout material obtained from laboratory tests are utilized. The applied material model as well as the suitable values of the compressive softening were validated using the experimental work of Anders 2007. Figure 19a shows the finite element model of the grouted connection. The blue elements represent the high strength concrete grout. On the in-

terior surface of the pile (diameter 3 m, thickness 50 mm) and on the exterior of the pin (diameter 2.2m, thickness 53 mm) the shear strength of the grout is improved by shear keys. In this particular case, the shear keys are created by welds with the dimension of 10x20 mm and the vertical spacing of 350 mm. The compressive strength of the grout is 80 MPa. The grouted connection design was verified by nonlinear analysis for ULS (ultimate limit state) and for FLS (fatigue limit state) by global approach based on nonlinear analysis. shows the typical cracking pattern in the grout for ULS analysis for the case with eccentric and inclined relative pile-pin position. The calculated load-displacement curves for few selected load cases are shown in Figure 21. In this project, the PSF approach was used for the global assessment for ULS and FLS. It can be observed that quite high safety margin (greater than 2.2) was obtained for almost all load cases. The standard design approach for the grouted connection for instance by EN ISO 19902 is based on empirical formulas that are derived from experimental results with limited validity. In GL guideline (2005) a very limited information is provided for finite element analysis. These standard approaches are typically based on checking admissible stress values, which is however impossible to do for the case of shear keys, where high stress concentration occurs. Therefore a global approach by nonlinear analysis is a very attractive and the most realistic method for the design of grouted connections with shear keys.

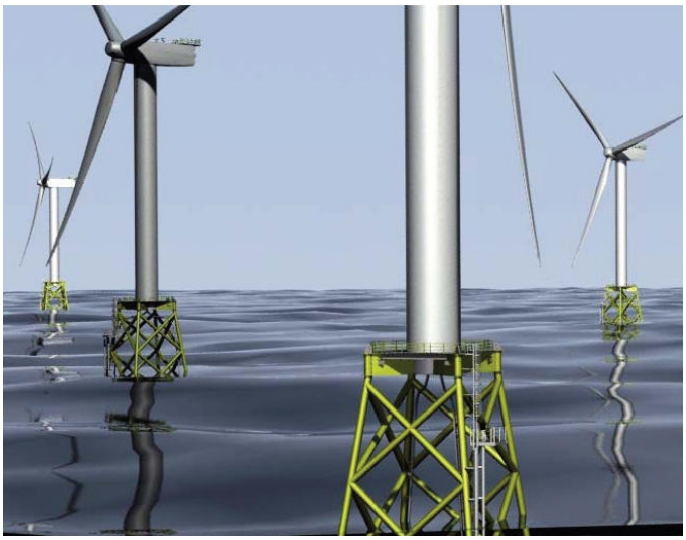

Figure 18. Typical configuration of off-shore wind farms.

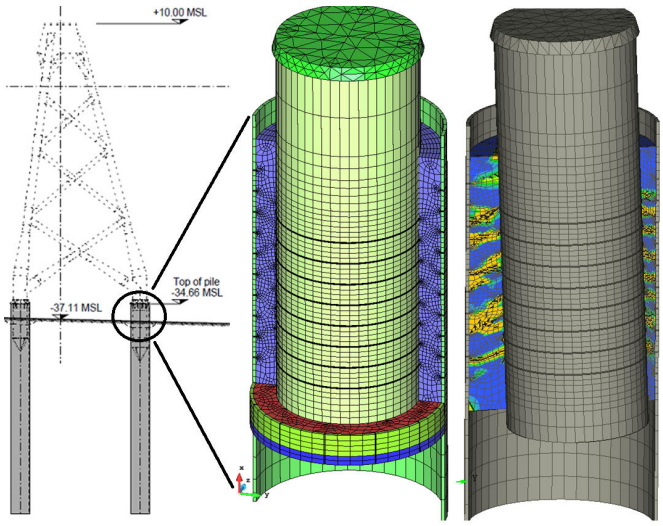

(a) (b) (c)

Figure 19. Grouted connection in a typical jacket supporting structure (a), finite element model including shear keys, (b) cracking pattern at ULS design load level (c).

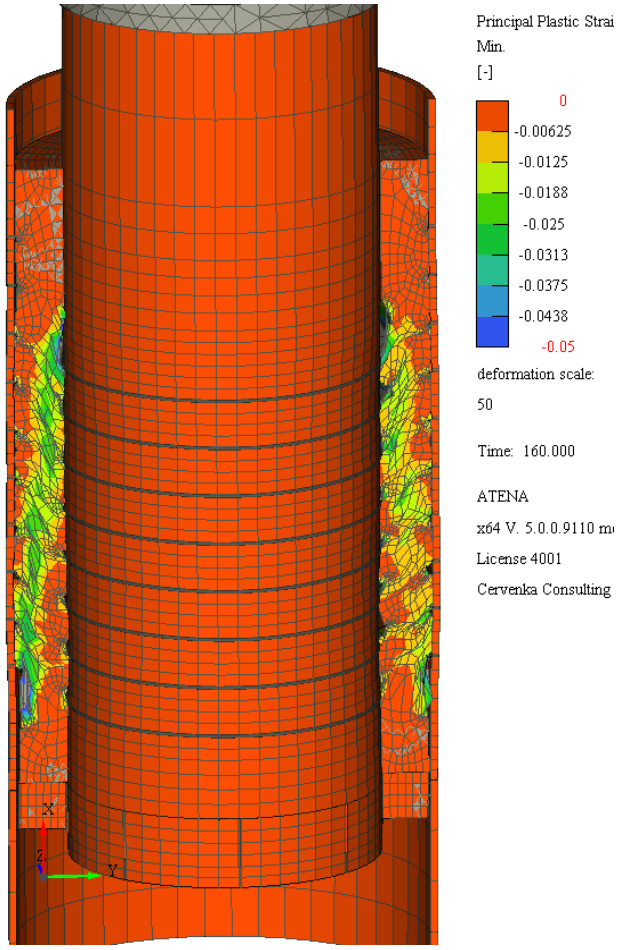

Figure 20: Crushing of concrete in the grouted connection at failure.

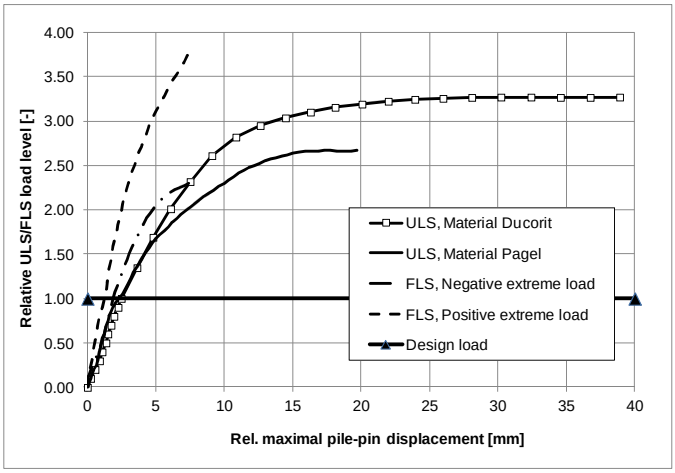

Figure 21: Load-displacement curves for grouted connection design for ULS/FLS based on global safety factor

6 CONCLUSIONS

The paper discusses the importance of suitable regularization technique to be used also for compressive softening. This is often neglected, although the proper modeling of concrete response in compression can be considered to be even more important in practical applications than the modeling of tensile cracking. This is mainly due to fact that the reinforced concrete design is based on ultimate limit states, where the full plasticization of concrete is assumed in compression with rather high values of compressive strains, typically up to 3,5‰.

The paper discusses a regularization technique for compression softening, which is analogical to the widely used crack band model in tension. The proposed parameter is called crush band, and depends on the finite element size in the direction of the minimal principal stress. The crush band should be however limited by some minimal value, which corresponds to the minimal size of the compression zone that can develop in the structure perpendicular to the direction of the acting minimal principal stress.

This approach was validated using uni-axial compression tests and by comparing results for the rotational capacity of reinforced concrete beams in flexure. The model is able to capture the main features, but proper investigation of the model uncertainties should be always performed when applying nonlinear analysis to practical engineering problems.

The presented approach was applied for checking the ultimate and fatigue limit states of the grouted connection in the offshore wind power generators.

The presented results are based on research performed within the project P105/12/2051 "Model uncertainties" from Czech science foundation and Eurostars project E!7521 SE-Lab. Authors gratefully acknowledge this support

7 REFERENCES

Anders, S. 2007. *Betontechnologische Einflüsse auf das Tragverhalten von Grouted Joints*, Dr. Ing. Dissertation, Universität Hannover

Bažant, Z.P. & Oh, B.H., 1983. Crack band theory for fracture of concrete. *Materials and Structures, RILEM* 16 (3), 155–177.

Bosco C. & Debenardi, P. G. 1993. Influence of some basic parameters on the plastic rotation of reinforced elements. Ductility requirements for structural Concrete - Reinforcement. Comite Eruo-international du Breton. CEB bulletin 218. pp25-44

Červenka, J., Červenka, & V., Eligehausen, R., 1998. Fracture-plastic material model for concrete. Application to analysis of powder actuated anchors. *Proceedings of the 3rd International Conference on Fracture Mechanics of Concrete Structures - FraMCoS 3, Gifu, Japan*, eds. H. Mihashi and K. Rokugo, Aedificatio Publishers, Freiburg, Germany, 1998, 2, 1107-1116.

Červenka J. & Papanikolaou V. 2008. Three Dimensional Combined Fracture-Plastic Material Model for Concrete. *Int Journal of Plasticity*. 24:2192-220.

Červenka, V., Červenka, J. & Jendele, L. 2013. *ATENA Program Documentation, Part 1: Theory, 2013*, Cervenka Consulting s.r.o., 2013, www.cervenka.cz

Červenka, V. 2013. Reliability-based non-linear analysis according to fib Model Code 2010, *Structural Concrete, Journal of the fib*, Vol. 14, March 2013, ISSN 1464-4177, pp. 19-28, DOI: 10.1002/suco.201200022.

Hordijk, D.D. 1991. *Local Approach to Fatigue of Concrete*. Ph.D. Thesis. Delft University of Technology.

Jendele, L. & Cervenka, J. 2006. Modelling Bar Reinforcement with Finite Bond, *Computers and Structures*, 84, 1780-1791

Menetrey, P. & Willam, K.J. 1995. Triaxial Failure Criterion for Concrete and its Generalization. *ACI Structural Journal*. 1995;92:311-8

Nakamura H. & Higai T. 2001. Compressive Fracture Energy and Fracture Zone Length of Concrete, *Modeling of Inelastic Behavior of RC Structures under Seismic Loads*, ASCE, pp.471-487.

Tatematsu H., Nakamura H. & Higai T. 1997. Experimental study on compressive fracture zone for concrete of Joint of RC column. *Proc. of JCI*, Vol.19, No.2, pp.897-903.

Van Mier, J.G.M., 1986. Multiaxial strain softening of concrete. Part I : Fracture. *Materials and Structures*, RILEM 19 (111), 179-190.